Effect of Antisite Defects on the Formation of Oxygen Vacancies in Sr2FeMoO6: Implications for Ion and Electron Transport

3 AUTHORS, INCLUDING:

Ana B Munoz-Garcia

University of Naples Federico II

29 PUBLICATIONS **294** CITATIONS

SEE PROFILE

Michele Pavone

University of Naples Federico II

58 PUBLICATIONS **1,183** CITATIONS

SEE PROFILE

# Effect of Antisite Defects on the Formation of Oxygen Vacancies in Sr$_2$FeMoO$_6$: Implications for Ion and Electron Transport

Ana B. Muñoz-García, Michele Pavone,[†] and Emily A. Carter*

Department of Mechanical and Aerospace Engineering, Program in Applied and Computational Mathematics, and Gerhard R. Andlinger Center for Energy and the Environment, Princeton University, Princeton, New Jersey 08544-5263, United States

ABSTRACT: To face worldwide energy-related environmental concerns, solid oxide fuel cell (SOFC) technology emerges as a promising route for clean and efficient production of electricity. Within this context, great efforts have been devoted to the development of SOFC devices able to run at intermediate temperatures and to retain electrochemical performance as good as in the high temperature regime. To this end, materials that have characteristics of mixed ionic and electronic conductors (MIECs) have been proposed as electrodes for SOFC applications. Among many proposed systems, MIEC electrodes based on strontium iron molybdenum oxide (Sr$_2$Fe$_{2-x}$Mo$_x$O$_{6-\delta}$) have been proven to be extremely efficient for intermediate temperature SOFC. However, to advance SFMO-based electrodes further, a detailed understanding of the physical and chemical processes involved and of the corresponding electronic and structural features is needed. As a first step in this direction, we investigate via quantum mechanics the Sr$_2$FeMoO$_6$ (SFMO) material, with a particular emphasis on characterizing the formation of bulk oxygen vacancies, which is a key component of the oxide ion diffusion process in SOFC electrodes. To explore the feasibility of vacancy formation in different local environments, we studied ordered SFMO as well as SFMO with Fe$_{Mo}$−Mo$_{Fe}$ antisite defects. The formation energy for oxygen vacancies along M−O−M′ bonds is predicted to follow the trend Fe−O−Fe < Fe−O−Mo < Mo−O−Mo. Therefore, oxygen diffusion should be enhanced for local higher concentrations of iron. Moreover, the reduced material may have enhanced electronic conductivity, as judged by its altered electronic structure. Our results and analysis of the reasons behind this trend highlight the importance of further experimental and theoretical investigations on Fe-rich SFMO-based materials.

KEYWORDS: solid-oxide fuel cells, oxygen vacancies, perovskites, antisite defects
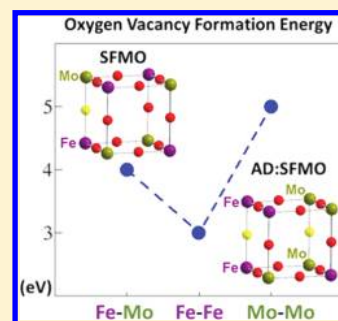
1. INTRODUCTION

Recent worldwide interest in renewable energy has refocused attention on solid oxide fuel cells (SOFCs), thanks to their ability to produce electricity in an environmentally friendly manner.[1] Fuel cells are devices that convert the chemical energy of fuels, such as hydrogen or methane, to electricity via electrochemistry.[2] Usually, the nature of the electrolyte names the type of fuel cell. SOFCs are characterized by the use of a solid oxide material as the electrolyte, which conducts oxygen anions from the cathode to the anode. A SOFC is made of three main layers, the anode (for fuel oxidation), the cathode (for oxygen reduction), and the electrolyte, plus an interconnect material. In state-of-the-art SOFCs, the electrolyte is a dense layer of ceramic that conducts oxygen ions. Its electronic conductivity must be kept as low as possible to prevent losses from leakage currents. The most common electrolyte materials are yttria-stabilized zirconia (YSZ) and gadolinium-doped ceria.[2−4] Electrode materials must be very porous to allow easy diffusion of the fuel and ideally must conduct both oxygen anions and electrons. The most common anode material is a composite made of Ni and YSZ. Either the anode or the electrolyte can be the thickest and strongest layer in a SOFC cell, providing the mechanical support. The cathode, also known as an air electrode, is a thin porous layer on the electrolyte where the oxygen reduction reaction (ORR) takes

place. Currently, lanthanum strontium manganite (LSM) is the cathode material of choice for commercial use because of its compatibility with doped zirconia electrolytes, stability at high temperature, ability to catalyze the ORR, reasonable electronic conductivity, adequate porosity, and low cost.[5] However, LSM is not a good ionic conductor and consequently the electrochemically active ORR is thought to occur only at the triple phase boundary, where the electrolyte, air, and cathode meet.[6]

The materials used in SOFCs become electrically and ionically active only at high temperatures, typically between 700 and 1000 °C. At these temperatures, SOFCs can convert a wide variety of fuels with good resistance to poisoning, which is a common problem with other fuel cell designs. Unfortunately, the high thermal stress results in premature aging of interconnect materials and an active research is devoted to finding new materials for intermediate temperature SOFCs that can run more efficiently within the 500−800 °C range. Unfortunately, reduction of the SOFC operating temperature inhibits the diffusion of O anions and consequently increases the polarization resistance, with this effect being more pronounced at the cathode where the
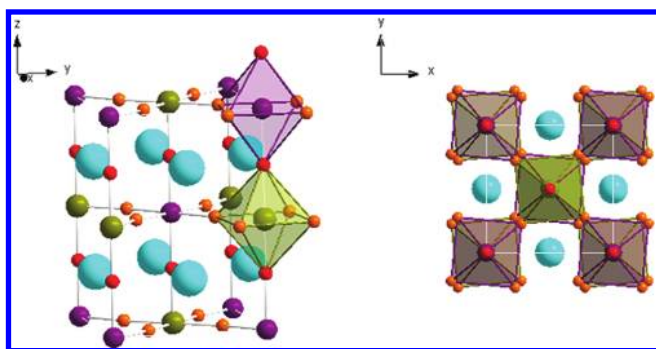
Figure 1. Left: $I4/m$ unit cell of Sr_2FeMoO_6. $Fe^{(3-\delta)+}$ ions and FeO_6 octahedra in purple, $Mo^{(5+\delta)+}$ ions and MoO_6 octahedra in olive green, Sr^{2+} ions in blue, and O^{2-} ions (O_I, red; O_{II}, orange) shown. Right: view along c axis, tilted octahedra shown.

ORR takes place. Therefore, great efforts have been devoted to finding cathode materials that possess the following properties: (1) good electronic conductivity; (2) good ionic diffusivity; (3) good catalytic activity for the ORR; and (4) a thermal expansion coefficient compatible with the electrolyte. The ideal material then should be a mixed ionic electronic conductor (MIEC).[7] Within this context, the development of innovative and efficient cathode materials has focused on strontium-doped lanthanum transition metal oxides ((La,Sr)MO₃, M = Mn, Fe, Co, Ni)[8,9] that present complex perovskite structures. The double perovskite $Sr_2Fe_{2-x}Mo_xO_6$ (SFMO) was proposed some time ago as a promising MIEC material,[10] its properties being very sensitive to (and thereby tunable via) the relative ratio of Fe:Mo ions.[11] In particular, recently $Sr_2Fe_{1.5}Mo_{0.5}O_{6-\delta}$ was used successfully both for the anode and the cathode in a symmetric SOFC,[12] which has the advantage of limiting thermal expansion mismatch inherent in the traditional SOFCs that utilize three different materials for the cathode, anode, and electrolyte.

Further developments of this new type of material call for a deeper understanding of its properties, especially how they can be optimized by varying the Fe:Mo ratio. With this in mind, we report a first-principles quantum mechanics study of the bulk properties of the parent double perovskite Sr_2FeMoO_6 in which the ratio of Fe:Mo is 1:1. In particular, we characterize the structural, electronic, and magnetic features of this material in its equilibrium structure and in the presence of defects, namely antisites and oxygen vacancies that are likely to form under SOFC operation. As we shall see, antisite defects form easily in Sr_2FeMoO_6 and their presence promotes oxygen vacancy formation, which is key to attaining good ionic conductivity.

Stoichiometric ordered double perovskites ($A_2BB'O_6$) possess a modified perovskite structure (ABO_3) where BO_6 and $B'O_6$ octahedra are arranged in two interleaving fcc sublattices. The A sites are occupied by alkaline or rare earth ions, while the B and B′ sites contain transition metal ions. Although this structure falls within the cubic Fm3m space group, it is very often distorted as a consequence of steric pressure and temperature variations. Because of the large size of Sr^{2+} ions in Sr_2FeMoO_6, the FeO_6 and MoO_6 octahedra undergo cooperative tilting distortions toward the most energetically favorable structure, which causes a symmetry reduction of the cubic cell to the tetragonal group $I4/m$ (Figure 1). Thus, the Sr_2FeMoO_6 crystal structure contains two formula units per unit cell, i.e., 20 atoms: two Fe atoms

placed in the (a) Wyckoff positions of the $I4/m$ cell, two Mo atoms in (b) sites, four Sr atoms in (d) sites and 12 O atoms in both 4(e) and 8(h) symmetry sites.[13]

Ferromagnetism arises in Sr_2FeMoO_6 from spin properties at Fe and Mo sites, which have nominal oxidation states of Fe(III) and Mo(V). In the high spin configuration, Fe^{3+} (d^5) has an $S_z = 5/2$ spin moment, whereas Mo^{5+} (d^1) bears an $S_z = 1/2$ spin moment. Within this ionic picture, and in analogy with the manganites, one can think of a bare antiferromagnetic (AF) interaction between neighboring Fe and Mo sites by means of their 5 μ_B/f.u. and -1 μ_B/f.u. respective spin moments. However, some SFMO properties cannot be explained by such a simple model.[14] Sarma et al.[15] proposed a model for magnetism in this compound arising from electron hopping interactions between Fe and Mo states with the same spin and orbital symmetry, which allows $Fe(3d_{t_{2g}})-O(2p)-Mo(4d_{t_{2g}})$ hybridization and, as a consequence, lowers the energy of the Mo spin down states, whereas the spin up states are pushed further up. This electron transfer results in a noninteger valence for both the cations, $Fe^{(3-\delta)+}$/$Mo^{(5+\delta)+}$, in agreement with Mössbauer and X-ray absorption experiments, as originally proposed by García-Landa et al.[16] Additionally, this feature also explains the half-metallic nature of the compound, as reported in the calculations of Kobayasi et al. based on density functional theory (DFT).[10]

Experiments have shown that such electronic and magnetic properties of perfect double perovskites significantly change upon the presence of antisite defects (ADs).[17] In SFMO, although the total Fe and Mo atomic concentrations are well controlled, it is much more difficult to control the distribution of Fe and Mo atoms in the two interleaving lattices during synthesis. In reality, all samples contain a certain amount of ADs, where some of the Fe atoms exchange positions with Mo atoms. Typically these ADs are randomly distributed and their number is characterized by the degree of Fe/Mo ordering of the sample, which can be probed by X-ray diffraction. Because of the similar ionic sizes of Fe and Mo (Fe^{3+} = 0.645 Å, Mo^{5+} = 0.61 Å in 6-fold coordination[18]), the degree of ordering in SFMO single crystals is not higher than 92% (i.e., the AD concentration is ∼8%).[19] The half-metallic character (and, in turn the electronic transport properties) are quite sensitive to the presence of ADs, because they modify the Fe−O−Mo bonding network thought to be responsible for electron hopping. Additionally, formation of oxygen vacancies (O*) in SFMO, corresponding to removal of neutral O atoms from the lattice, alters the number of delocalized electrons and also affects the magnitude of the magnetic moments of surrounding atoms.

Antisite and cation-excess defects in bulk SFMO were discussed in detail in a recent study by Windl and co-workers,[20] by means of a generalized gradient approximation (GGA)+U approach very similar to ours. They address mainly the subtle effects of such defects on electronic and magnetic features, within the framework of possible application of SFMO-based materials as high temperature ferromagnets. Windl and co-workers' results highlight very interesting features of antisite or cation-excess defects that affect the half-metallic nature of SFMO.

Complementary to these findings, here we present an in-depth investigation of the properties of bulk SFMO with and without ADs and upon formation of oxygen vacancies. In AD-free SFMO, oxygen vacancies involve only Fe−O−Mo-type bonds. However, in AD:SFMO, oxygen vacancies can also occur along Fe−O−Fe and Mo−O−Mo bonds. Insight into the likelihood of formation of these different types of vacancies and their role in

tuning the magnetic and electronic properties of bulk SFMO is then of great interest in the context of SOFCs.

2. METHODS AND COMPUTATIONAL DETAILS

All calculations reported in this work were carried out using the VASP code (version 5.2.2).[21] We started by characterizing defect-free Sr_2Fe-MoO_6 using methods based on spin-polarized DFT. Thanks to its effective balance of accuracy and feasibility, DFT has become the most common framework for studying the electronic structure of materials. However, the self-interaction error (SIE) that arises from the approximate forms of exchange-correlation density functionals produces especially large errors in mid-to-late first row transition metal oxides, due to the large number of large (~ 1 eV) intra-atomic exchange interactions felt by electrons in very tightly localized d-orbitals in these multiply-charged cations. To eliminate much of the SIE, we employ the DFT+U method.[22] This approach applies an on-site potential at atom positions and requires a parameter, U-J, which is the difference between the average Coulomb and exchange energy felt by electrons localized on the same atom with the same angular momentum. While frequently effective, this method often retains empiricism in the choice of the U-J, parameter. Instead, we use a recently developed ab initio scheme to calculate U-J,[23] that has been successfully validated on chromium and iron oxides. In this work, because of the presence of d electrons in Fe and Mo atoms, we tested not only DFT but also DFT+U approaches, with local (the local density approximation, LDA)[24] and semilocal (the Perdew–Burke–Ernzerhof, PBE, version of the GGA)[25] exchange-correlation density functionals.

Regarding the DFT+U approach used in this work, d shells on Fe and Mo have to be accounted for simultaneously and, thus, in principle, two (U-J) parameters should be chosen. In Fe, the 3d electrons are strongly localized and give rise to the gap in the α spin-channel of this half-metallic compound. Therefore, apart from the standard pure DFT with (U-J)$_{Fe}$ = 0 eV, we checked Sr_2FeMoO_6 bulk and magnetic properties for the following set of (U-J)$_{Fe}$ values: 3.7 and 4.3 eV (corresponding to the ab initio values for Fe^{2+} and Fe^{3+}, respectively[23b]) and the average between them (4.0 eV). Considering the intermediate $Fe^{(3-\delta)+}$ valence and the negligible variation of the Sr_2FeMoO_6 properties examined, the average value of (U-J)$_{Fe}$ = 4.0 eV is our choice in this work. In contrast to the Fe electronic structure, the metallic character of the beta spin-channel of this compound has been attributed mostly to a delocalized d electron of Mo,[15,16,20,26–29] which can be viewed as $Mo^{(5+\delta)+}$. For this reason, Mo is expected to be accurately described within a pure DFT framework and no (U-J)$_{Mo}$ is in principle needed. In fact, calculations performed for SFMO while varying the value of (U-J)$_{Mo}$ with fixed (U-J)$_{Fe}$ = 4 eV confirm that no (U-J)$_{Mo}$ is needed and in fact its use worsens the good properties predicted with (U-J)$_{Fe}$ = 4 eV and (U-J)$_{Mo}$ = 0 eV values.

The core electrons on each atom were treated as a frozen atomic core according to the projector-augmented wave (PAW) method.[30] Among the available PAW potentials supplied with the VASP code, we used the only one available for Sr, which leaves ten electrons in the outer core/valence ($4s^2$, $4p^6$, and $5s^2$) to be optimized self-consistently. For oxygen, there are three different potentials, all acting on the same number of valence electrons ($2s^2$ and $2p^4$), but with different core radii: a soft potential with a large core radius (O_s), an intermediate one (O), and a hard potential (O_h); we used the intermediate (O) as the best compromise between accuracy and cost. For Fe, we tested PAW potentials acting on eight ($4s^2$ and $3d^6$) or 14 ($3p^6$, $4s^2$, and $3d^6$) outer core/valence electrons and for Mo, we tested the six ($5s^2$ and $4d^4$) and 12 ($4p^6$, $5s^2$, and $4d^4$) outer core/valence electron PAW potentials. No significant differences in the prediction of Sr_2FeMoO_6 properties were found with the more demanding Fe and Mo PAW potentials, so we used the standard potentials for Fe and Mo, with eight and six valence electrons, respectively.

The outer core/valence electron PAW-DFT pseudowave functions were expanded in a planewave basis, with a kinetic energy cutoff of 800 eV and a k-point sampling based on the Monkhorst–Pack[31] scheme ($6 \times 6 \times 4$ for the Sr_2FeMoO_6 20-atom tetragonal cell; $4 \times 4 \times 4$ for the 40-atom pseudocubic one). These parameters ensured convergence of the computed total energy to within 1 meV per formula unit for SFMO.

We calculated the lattice parameters of the tetragonal unit cell of the perfectly ordered SFMO by relaxing both ion positions and cell volume and shape until the total force on each atom was <0.01 eV/Å. The bulk modulus was then calculated from the Murnaghan equation of state.[32] Atom- and angular momentum-projected densities of states (PDOS) and magnetic moments were obtained as direct output of the VASP code.[21] Topological analysis of the electron density was carried out employing the Bader approach.[33] The electron density difference isosurface was computed from the density of the vacancy defect system plus the spherically averaged density of an isolated gaseous nonmagnetic oxygen atom placed at the vacancy position, minus the density of the perfect bulk crystal (no vacancy). The plots were created with the VESTA program.[34]

The AD formation energy was computed according to the following process:

$$Sr_8Fe_4Mo_4O_{24} \rightarrow AD{:}Sr_8Fe_4Mo_4O_{24}$$
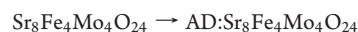
The O vacancy formation energy was computed in the standard way, with respect to a free oxygen molecule in its triplet state, according to the processes:

$$Sr_8Fe_4Mo_4O_{24} \rightarrow Sr_8Fe_4Mo_4O_{23} + 1/2\,O_2$$

and

$$AD{:}Sr_8Fe_4Mo_4O_{24} \rightarrow AD{:}Sr_8Fe_4Mo_4O_{23} + 1/2\,O_2$$

for the perfectly ordered SFMO and SFMO with ADs, respectively.

3. RESULTS AND DISCUSSION

3.1. Defect-Free SFMO. First, we discuss the magnetic arrangement of Fe and Mo within the tetragonal Sr_2FeMoO_6 unit cell. The experimental value of the total magnetization of 3.5–4.0 μ_B/f.u. and former investigations of this material[10,14,15] suggest the iron to be in a high spin configuration. Full relaxation of both lattice vectors and atomic positions were performed without any symmetry constraints and starting from different relative magnetic configurations between iron and molybdenum ions: (a) Fe^{3+} and Mo^{5+} species ($S = 5/2$ and $S = 1/2$, respectively) with spins antiferromagnetically aligned, (b) all species with spins ferromagnetically aligned, and (c) considering the limit of Fe^{2+} and Mo^{6+} ($S = 2$ and $S = 0$, respectively). From all these initial configurations, the LDA and PBE density functionals both predict a nonmagnetic solution. These results are in contrast with experimental observations and prove that pure DFT should not be used for describing SFMO. With DFT+U, all the initial magnetic configurations converged to the same AF state; the non-magnetic arrangement was predicted to be higher in energy than the AF state by ~ 1.0 and ~ 1.6 eV, at the ab initio LDA+U and PBE+U levels of theory, respectively. Moreover, the ferromagnetic (FM) alignment of all Fe ions on the Fe sublattice is found to be the most stable compared to all AF ones tested, by more than ~ 130 meV. The most stable Fe–Mo AF arrangement predicted by ab initio DFT+U theory is compatible with the model of Sarma et al.[15] In particular, the AF configuration is the only one that allows the down-spin Mo $4d_{t_{2g}}$ electron to delocalize onto the empty down-spin Fe $3d_{t_{2g}}$ orbitals, consistent with the $Fe^{(3-\delta)+}$/$Mo^{(5+\delta)+}$ valence.

Table 1. DFT and DFT+U Properties of Defect-Free Sr_2FeMoO_6 (SFMO; Figure 1) in Its Ground State with Fe and Mo Magnetic Moments Antiferromagnetically Aligned[a]

Property	Expt.	LDA+U		PBE+U	
		$(U\text{-}J)_{Fe}= 0$ eV	$(U\text{-}J)_{Fe} = 4$ eV	$(U\text{-}J)_{Fe}= 0$ eV	$(U\text{-}J)_{Fe} = 4$ eV
$a\ (= b)$ (Å)	5.55215^c	5.39	5.48	5.52	5.61
c (Å)	7.90134^c	7.63	7.87	7.81	8.03
V_{cell} (Å³)	243.570^c	221.95	236.04	237.79	252.44
$z(O_I)$	0.2542^c	0.2465	0.2531	0.2488	0.2544
$x(O_{II})$	0.2767^c	0.2560	0.2892	0.2589	0.2882
$y(O_{II})$	0.2266^c	0.2370	0.2160	0.2387	0.2201
$d(Fe-Mo)_{xy}$ (Å)	3.926	3.81	3.87	3.90	3.96
$d(Fe-Mo)_z$ (Å)	3.951	3.81	3.93	3.90	4.01
$d(Fe-O)$ (Å)	$2.009(\times2)^b$	$1.88(\times6)$	$1.99(\times2)$	$1.94(\times6)$	$2.04(\times2)$
	$1.986(\times4)^c$		$1.98(\times4)$		$2.03(\times4)$
$d(Mo-O)$ (Å)	$1.942(\times2)$	$1.93(\times6)$	$1.94(\times6)$	$1.96(\times6)$	$1.97(\times6)$
	$1.960(\times4)^c$				
$\alpha(Fe-O-Mo)_{xy}$ (deg)	169^c	176	163	175	164
$\alpha(Fe-O-Mo)_z$ (deg)	180^c	180	180	180	180
B (GPa)	266^d	218	183	170	153
$M(Fe)$ (μ_B)	$4.0-4.1^{e,f,g,h}$	0.0	4.0	0.0	4.1
$M(Mo)$ (μ_B)	-0.2 to $-0.5^{e,f,g,h}$	0.0	-0.4	0.0	-0.5
M_s/f.u. (μ_B)	$3.5-4.0^{e,f,g,h}$	0.0	3.8	0.0	3.9
gap (α) (eV)	0.5^i, 1.3^j	0.48	1.84	0.43	2.24
gap (β) (eV)	$0.0^{i,j}$	0.48	0.00	0.43	0.00

^{a} Lattice vectors (a, b, and c); cell volume (V_{cell}); internal positions ($z(O_I)$, $x(O_{II})$, $y(O_{II})$); Fe—Mo distances (in the xy plane ($d(Fe-Mo)_{xy}$) and along the z axis ($d(Fe-Mo)_z$): distances Fe—O ($d(Fe-O)$) and Mo—O ($d(Mo-O)$) in the FeO_6 and MoO_6 pseudooctahedra; Fe—O—Mo angles in the xy plane ($\alpha(Fe-O-Mo)_{xy}$) and along the z axis ($\alpha(Fe-O-Mo)_z$); bulk modulus (B); magnetic moments on Fe ($M(Fe)$) and Mo ($M(Mo)$) atoms and total magnetization per formula unit (M_s); and eigenvalue gaps of the spin up (gap (α)) and spin down (gap (β)) channels. ^{b} ($\times N$) gives the number N of oxygen atoms at the distance listed. References to experimental values: ^{c} From ref 13 (70 K). ^{d} From ref 49 (r.t.). ^{e} From ref 35 (5 K). ^{f} From ref 16 (2 K). ^{g} From ref 50 (10 K). ^{h} From ref 10 (4.2 K). ^{i} From ref 19 (10 K). ^{j} From ref 51 (20 K).

Table 1 lists calculated Sr_2FeMoO_6 bulk properties in comparison to experimental values. From these data, we observe very different behavior predicted by DFT versus DFT+U, regardless of the exchange-correlation flavor.

Despite reasonable reproduction of the structural properties of Sr_2FeMoO_6, pure DFT completely fails to describe its magnetic properties (vide supra) and electronic structure. In addition to the incorrect prediction of a nonmagnetic ground state ($M_s = 0$), DFT predicts a symmetric electronic structure for the α and β spin-channels, leading to the prediction of Sr_2FeMoO_6 to be a semiconductor (Figure 2a,b), in contrast with its known half-metallic nature. Consequently, no further calculations were carried out at the pure DFT level of theory.

LDA+U and PBE+U, with the ab initio-derived U-J value for Fe, both predict SFMO lattice constants and interatomic distances (Fe—Mo, Fe—O, Mo—O) within ~1% of experiment. Errors in computed cell volume (within ~3% of experiment) and interatomic distances all show a consistent and familiar trend going from LDA+U to PBE+U. LDA+U-predicted values are slightly underestimated (as expected for LDA exchange-correlation), whereas the PBE+U ones are off in the opposite direction but to a similar extent. Also, the predicted angles are close to the experimental counterparts.

On the other hand, the SFMO bulk modulus (B) is not properly described, even by adding the U-J term to LDA and PBE density functionals. This breakdown comes from the improper description of long-range electronic correlation within

approximate DFT. Local and semilocal approximations do not include the physics of dispersion forces. These are long-range attractive interactions that have a key role in determining macroscopic mechanical properties of molecular crystals and those containing interacting polyhedra, which is likely why our DFT-based predictions of the SFMO B are lower than the experimental values.

Regarding the electronic structure, despite overestimating the α-gap value, DFT+U provides a good description of the half-metallic character (Table 1 and Figure 2c,d) as well as of the total magnetization and the magnetic moments on iron and molybdenum compared to experimental data[17,19,35] and to previous calculations.[10,15,36–39] The Fermi level in SFMO is predicted by DFT+U to be at the band formed mostly by $Fe(3d_{t_{2g}} \downarrow)$ and $Mo(4d_{t_{2g}} \downarrow)$ sub-bands, responsible for the electron hopping. In the spin up band, the top of the valence band has a $Fe(3d_{e_g} \uparrow)-O(2p)$ mixed character, whereas the bottom of the conduction band is dominated by $Mo(4d_{t_{2g}} \uparrow)$ states, with a small $O(2p)$ contribution.

Overall, LDA+U and PBE+U predictions are both in qualitative agreement with available experimental data. However, in the following we choose to report only PBE+U results because we are mostly concerned with modeling oxygen vacancy defects. From a general perspective, the PBE exchange-correlation functional performs much better than the LDA in describing (a) the breaking of a transition-metal oxygen bond and (b) the electronic structure of the triplet ground state of O_2,[40] both of which are
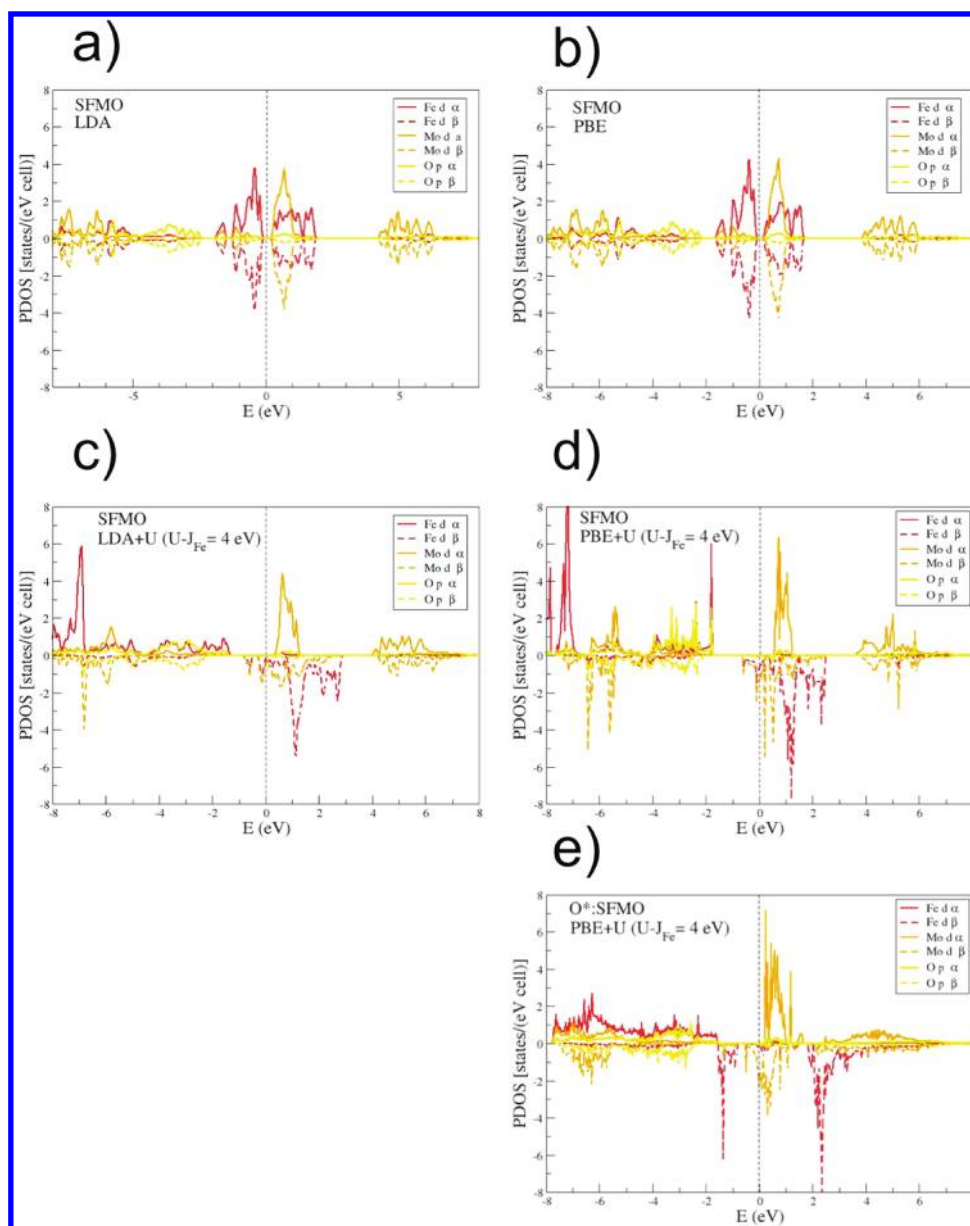
Figure 2. Projected densities of states (PDOS) of SFMO predicted by various levels of theory: (a) DFT-LDA, (b) DFT-GGA (PBE), (c) LDA+U, and (d) PBE+U. (e) PBE+U PDOS of O*:SFMO . $(U\text{-}J)_{Fe}$ = 4 eV in all DFT+U calculations. PDOS on Fe(d), Mo(d), and O(p) orbitals are shown. Positive values of PDOS refer to α-spin electrons whereas negative values refer to β-spin electrons. The DFT energies are shifted such that the Fermi energy (highlighted by a dashed line) is set to be zero.

related to the process of forming an oxygen vacancy, as discussed below in section 3.3.

3.2. Antisite Defects. When SFMO contains ADs, some Fe occupy Mo sites (Fe_{Mo}) and the same number of Mo atoms occupy Fe sites (Mo_{Fe}), which produce new Fe_{Mo}−O−Fe and Mo_{Fe}−O−Mo bonds as a consequence of this disorder.

The measured total saturation magnetization of SFMO has been interpreted as being due to the presence of these kinds of ADs in which the two newly neighboring Fe_{Mo} and Fe atoms present an FM alignment.[17] All-electron pure DFT-GGA (LMTO-ASA-GGA calculations of Saha-Dasgupta et al.[41] and FLAPW-GGA calculations of Stoeffler et al.[36,42]) bear out this FM picture. By contrast, TB-LSDA calculations of Solovyev et al. predict a coexistence of the FM and AF Fe_{Mo}−Fe spin arrangements[43] and Monte Carlo simulations of Ogale et al.[44]

and the already-mentioned GGA+U calculations by Windl and co-workers[20] find a clear preference for the AF situation. Given these disagreements in past work, we have studied both the FM and AF relative Fe_{Mo}−Fe spin arrangements, targeting not only the description of stoichiometric AD:SFMO in these two different relative spin orientations, but also the nature of oxygen vacancies that can be formed along Fe_{Mo}−O−Fe bonds with Fe_{Mo} and Fe cations FM and AF aligned. We have also considered two different situations within the Fe_{Mo}/Fe AF case: Mo_{Fe} with an initial spin of $S = 1/2$ or $S = -1/2$. These two initial spin configurations converge to the same ground state, with spin down magnetic moment on Mo_{Fe}. This behavior is consistent with the delocalized nature of the d electrons of Mo that can be achieved only in the spin down channel.
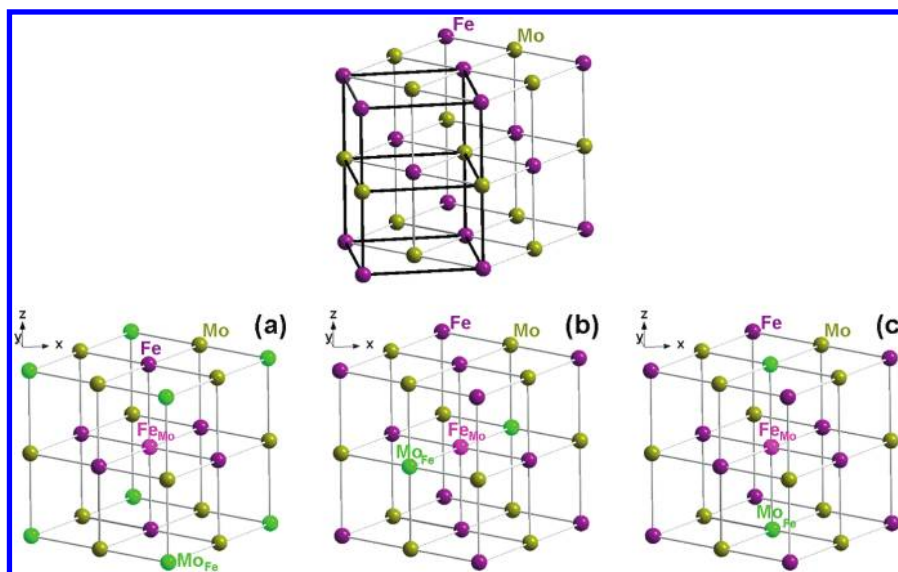
Figure 3. Top: Representation of interleaving Fe (purple) and Mo (olive green) sublattices of the tetragonal unit cell of SFMO (black lines, 2 Sr_2FeMoO_6 f.u.) and the corresponding $\sqrt{2} \times \sqrt{2} \times 1$ pseudocubic SFMO supercell (gray lines, 4 Sr_2FeMoO_6 f.u.). Bottom: Representation of the three different Fe_{Mo}(pink)$-Mo_{Fe}$(green) ADs in pseudocubic SFMO: (a) AD on the diagonal of the pseudocubic sublattice. (b) AD in the xy plane. (c) AD along the z axis. The oxygen atoms are not shown for ease of viewing.

To study SFMO with ADs, we analyzed a hypothetical model in which the ADs are ordered in a $\sqrt{2} \times \sqrt{2} \times 1$ pseudocubic SFMO supercell, that contains four Sr_2FeMoO_6 formula units and fulfills $a = b < c$ (Figure 3, top). The pseudocubic supercell vectors and atomic positions were generated from optimized parameters of tetragonal SFMO calculated at the PBE+U level of theory. Relaxation of the lattice parameters after creating an AD, with or without fixed cell shape, leads to a maximum difference of 0.010 Å in the lattice vectors and a negligible change in the cell shape, which remains pseudocubic with a/c ratios between 1.003 and 1.020 (Expt. 1.006). Consequently, we used the lattice vectors optimized for the perfectly ordered SFMO crystal and kept them fixed in the study of ADs, while relaxing the ion positions upon creation of an AD. Only one pair of Fe and Mo was exchanged at a time, leading to an ordering degree of 75% (ADs ~25%), lower than the maximum ordering observed experimentally. Nevertheless, these calculations provide useful information about the local properties around the defects, as well as setting a reference for the study of SFMO with both ADs and oxygen vacancies.

Three different AD $Fe_{Mo}-Mo_{Fe}$ have been considered because of the pseudocubic character of the supercell. They are shown in Figure 3 (bottom) and correspond to Fe_{Mo} and Mo_{Fe} exchanged along the diagonal of the cube formed by the four Fe and four Mo atoms (antisite a), exchanged along the x (or equivalently y) direction in the xy plane (antisite b), and along the z axis (antisite c). In this way the overall stoichiometry and the Fe:Mo ratio was kept 1:1 within the pseudocubic supercell.

Table 2 lists some of the property predictions for the different ADs. In all three ADs studied, the AF $Fe_{Mo}-Fe$ arrangement is significantly lower in energy than the FM one, in agreement with Windl and co-workers,[20] so that from now on within this section we discuss only our results for the AF case. The predicted energies of formation of the three ADs are all quite similar and moderate in magnitude (~0.4–0.7 eV), as expected considering the similar size of the $Mo^{5+/6+}$ and $Fe^{2+/3+}$ ions.[18] The diagonal AD is predicted to be the most favorable. The formation energies

of ADs along the xy plane and z directions are very similar, in accordance with the fact that in the pseudocubic cell $a \approx c$.

Comparison of the PBE+U $((U-J)_{Fe} = 4$ eV$)$ bond lengths in Tables 1 and 2 reveal that distances between Fe_{Mo} and Mo_{Fe} do not change substantially (to within 0.01 Å) compared to defect-free SFMO Fe–Mo distances. Structural parameters within the new $Fe_{Mo}O_6$ and $Mo_{Fe}O_6$ moieties also do not change significantly (to within 0.01/0.03 Å for Fe/Mo) with respect to their defect-free SFMO counterparts. The total magnetization (M_s) of the AD states are significantly lower than in the structure without ADs, as expected from the new AF-coupled $Fe_{Mo}-Fe$. The magnetic moment of ions at the AD sites are predicted to range from −4.1 to −4.2 μ_B for Fe antisites and from −0.5 to −0.9 μ_B for Mo antisites, the latter being similar to the defect-free case. No trend can be highlighted from these results; however clearly a significant rearrangement of the electronic degrees of freedom takes place at the AD sites. As a matter of fact, the electronic structures of AD:SFMO compounds appear to be quite different from the parent SFMO. PBE+U predicts very low eigenvalue gaps (DFT gaps referred to as eigenvalue gaps instead of band gaps, as they do not correspond to an observable, but rather as energy gaps between the lowest unoccupied and the highest occupied eigenstates): from zero to a maximum of 0.25 eV. Regardless of which AD is considered, the presence of ADs jeopardizes the half-metallic character of defect-free SFMO. Such different behavior is consistent with the fact that the Fe–O–Mo network is strongly modified by the presence of ADs. Beyond this, we can state that the particular electronic features of each AD may correspond to an artifact of our periodically ordered model whereas we would expect a disordered arrangement in real samples.

3.3. Oxygen Vacancy Defects. Diffusion of oxygen anions is a mandatory capability for effective SOFC electrode materials. Oxygen anions are too large to diffuse in the interstices of the lattice, so oxygen vacancies in the lattice must be formed in order for diffusion of such anions to occur (so that they may hop between empty sites). Consequently, a first estimate of how good

4530

dx.doi.org/10.1021/cm201799c |*Chem. Mater.* 2011, 23, 4525–4536

Table 2. DFT-PBE+U $((U\text{-}J)_{Fe} = 4$ eV) properties of SFMO containing antisite defects (ADs)^a

Fe/Fe$_{Mo}$	AD:Sr$_8$Fe$_4$Mo$_4$O$_{24}$(AD:SFMO)					
	(a)		(b)		(c)	
	FM	AF	FM	AF	FM	AF
E_f (eV)	1.00	0.42	0.84	0.63	0.93	0.67
d(Fe$_{Mo}$–Mo$_{Fe}$) (Å)	6.90^b	6.90^b	3.96	3.96	4.01	4.01
d(Fe$_{Mo}$–O) (Å)	2.04(×2)^c	2.06(×2)	2.02(×4)	2.06(×2)	2.07(×2)	2.07(×2)
		2.02(×4)	2.03(×2)	2.03(×2)	2.01(×4)	2.01(×4)
	2.02(×4)		2.01(×2)	2.01(×2)		
d(Mo$_{Fe}$–O) (Å)	2.01(×4)	2.01(×4)	2.01(×2)	2.01(×2)	2.00(×4)	2.00(×4)
	2.00(×2)	2.00(×2)	2.00(×2)	2.00(×2)	1.94(×2)	1.94(×2)
			1.94(×2)	1.94(×2)		
α (Fe–O–Fe$_{Mo}$)$_{xy}$ (deg)	170	171	166	166	168	169
α (Fe–O–Fe$_{Mo}$)$_z$ (deg)	180	180	180	180		
α (Mo–O–Mo$_{Fe}$)$_{xy}$ (deg)	164	165	165	165	164	164
α (Mo–O–Mo$_{Fe}$)$_z$ (deg)	180	180	180	180		
M(Fe$_{Mo}$) (μ_B)	4.31	−4.11	3.84	−4.17	4.14	−4.15
M(Fe^d) (μ_B)	4.21	4.15	4.22	4.05	4.20	4.00
M(Mo$_{Fe}$) (μ_B)	−0.55	−0.45	−0.83	−0.85	−0.33	−0.76
M(Mo^d) (μ_B)	−0.19	−0.18	−0.30	−0.36	−0.55	−0.45
M_s/f.u. (μ_B)	4.46	2.06	4.07	1.63	4.11	1.67
gap (α) (eV)	0.19	0.00	0.25	0.25	0.28	0.05
gap (β) (eV)	0.19	0.00	0.00	0.00	0.00	0.16

^{a} AD formation energies, E_f; structural parameters and magnetic properties (see definitions in Table 1) of the Fe$_{Mo}$ and Mo$_{Fe}$ atoms involved in the AD; and eigenvalue gaps of the α and β channels of AD:SFMO. Labels (a), (b), and (c) refer to the AD models of Figure 3, where the Fe and Mo magnetic moments are always preferentially aligned antiferromagnetically and the Fe$_{Mo}$ ADs are aligned either ferromagnetically (FM) or antiferromagnetically (AF) with respect to regular Fe atoms. ^{b} This distance in defect-free SFMO (pseudocubic cell) at the PBE +U level of theory is 6.89 Å. ^{c} (×N) reads for the number N of oxygen atoms at the considered distance. ^{d} Average value of the three transition metal ion sites not involved in the AD.
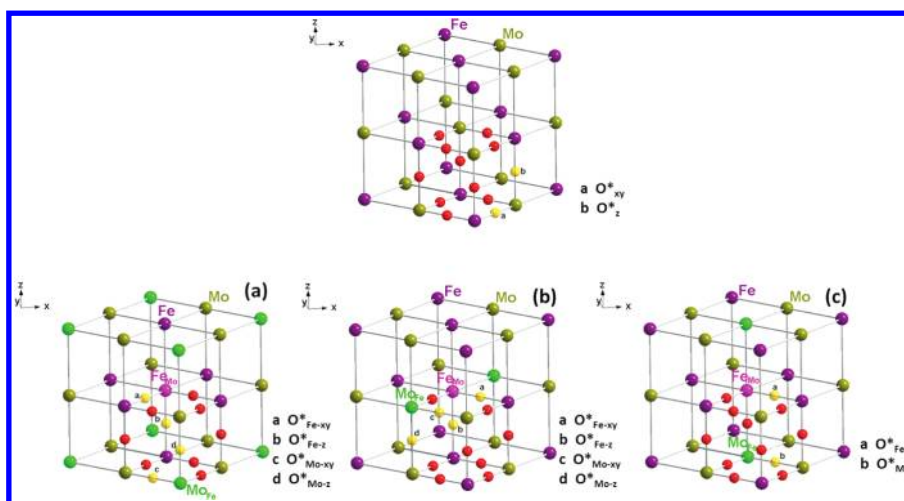

Figure 4. Top: Representation of the two different oxygen vacancies (O*) in SFMO: (a) Fe–O*–Mo in the xy plane (O*$_{xy}$) and (b) Fe–O*–Mo along the z axis (O*$_z$). Bottom: Representation of the Fe–O*–Fe and Mo–O*–Mo oxygen vacancies studied for the three (a–c) AD:SFMO of Figure 3: (a, b): Fe$_{Mo}$–O*–Fe in the xy plane (O*$_{Fe–xy}$), Fe$_{Mo}$–O*–Fe on the z axis (O*$_{Fe–z}$), Mo–O*–Mo in the xy plane (O*$_{Mo–xy}$), and Mo–O*–Mo on the z axis (O*$_{Mo–z}$). (c) Fe–O*–Fe (O*$_{Fe}$) and Mo–O*–Mo (O*$_{Mo}$). Oxygen atoms are shown in red, oxygen vacancies in yellow.

SFMO-based materials could be as ionic conductors can be drawn from the cost to form oxygen vacancies. In this work, we modeled Sr$_2$FeMoO$_{6-\delta}$ materials with δ = 0.25, by removing one oxygen atom from the Sr$_8$Fe$_4$Mo$_4$O$_{24}$ pseudocubic supercells represented in Figure 3, both defect-free and containing ADs. The strong sensitivity of oxygen vacancies to synthesis conditions leads to a great variability of experimentally reported oxygen vacancy concentrations. The value δ = 0.25 (~4%) studied in this work lies within the reported range of experimental O* concentrations: from δ = 0.03[45] to δ = 0.36.[46]

From AD-free SFMO, we created oxygen vacancies (O*) along the Fe–O–Mo bonds in the xy plane and along the z axis.

For SFMO with ADs, we studied all possible $Fe_{Mo}-O^*-Fe$ and $Mo_{Fe}-O^*-Mo$ vacancies. Figure 4 depicts schematically all oxygen vacancies considered. After removal of a neutral O atom, the electronic density was optimized and all nuclear positions were allowed to relax. For AD-free SFMO with one oxygen vacancy, we performed preliminary calculations relaxing also the lattice vectors together with the nuclear positions. We found a maximum increase of +1% in SFMO lattice constants together with a maximum decrease in the formation energy of O^* of 0.1 eV. This value is quite low by comparison to the magnitude of O^* formation energies (3–5 eV) so that we consider the vacancy concentration low enough to keep the crystal fixed at constant volume according to the lattice parameters optimized for the perfect SFMO structure.

The first event to occur after removal of a neutral oxygen atom is a reorganization of the electronic structure. Qualitatively useful initial insight into this process was obtained by computing effective Bader charges. Table 3 lists the predicted charges of Fe and Mo in defect-free SFMO, together with the ones at Fe and Mo AD sites in the three AD:SFMOs, before and after formation of an oxygen vacancy (O^*). The absolute values of Bader charges in all cases are lower than expected by considering standard ion valencies. This is consistent with the fact that the bonds in perovskite transition metal oxides are not purely ionic. In fact, the analysis of Bader charges can be safely used to qualitative estimate the amount of covalency involved in the chemical bond under investigation.

For defect-free SFMO at the PBE+U level of theory, the Bader charges are 1.61e for Sr, −1.15e and −1.17e for the two types of oxygen atoms, and 1.65e and 2.22e for Fe and Mo, respectively. The Sr cation has the most ionic character (relative to its formal oxidation state of +2) whereas the effective charges of Fe and Mo, which are much lower than $(3-\delta)^+$ and $(5+\delta)^+$, respectively, indicate a considerable amount of covalency exists in the Fe−O and Mo−O bonds. Such covalent picture is consistent with the computed PDOS (Figure 2) where the overlap between O and Fe states (α channel), and O, Fe, and Mo states (β channel), both below and above the Fermi level, indicates bonding and antibonding covalent character. This result is also in agreement with the aforementioned hopping model proposed for understanding the half-metallic nature of this material.

Based on the Bader charge on oxygen given above in the defect-free material, the formation of an oxygen vacancy calls for compensation of an effective negative charge of approximately −1.16e. For O^*:SFMO, the computed Bader charges provide similar pictures for the two vacancies O^*_{xy} and O^*_z: approximately −0.3e is donated to the Fe closest to the O vacancy, approximately −0.5 to −0.7e is distributed among the other iron ions, with the Mo closest to the vacancy and the Sr ions playing a very marginal role. The charge at Sr is not affected by either ADs or oxygen vacancies. Because of the vacancy, all remaining oxygen atoms reorganize their charge but do not receive significantly new charge, bearing a charge between −1.04e and −1.23e. Overall, the iron atoms received most of the charge left behind by the neutral oxygen. Such behavior is clearly depicted in electron density difference plots shown in Figure 5 and is consistent with the computed Bader charges listed in Table 3. From another perspective, the formation of an oxygen vacancy implies a reduction of the other remaining species. Our results suggest that within the AD-free SFMO environment, iron is the most likely to reduce its valence by accepting electrons into its d-orbitals.

Table 3. DFT-PBE+U ($(U-J)_{Fe}$= 4 eV) Effective Bader Charges of Fe and Mo Atoms in Defect-Free Sr_2FeMoO_6 (SFMO, $Sr_4Fe_2Mo_2O_{12}$, Figure 1); SFMO containing an oxygen vacancy (O^*:SFMO, $Sr_8Fe_4Mo_4O_{23}$, Figure 4 (top)); SFMO with an $Fe_{Mo}-Mo_{Fe}$ Antisite Defect (AD:SFMO, AD: $Sr_8Fe_4Mo_4O_{24}$, Figure 3 (bottom)); and SFMO with an Antisite Defect and an Oxygen Vacancy (AD,O^*:SFMO, AD: $Sr_8Fe_4Mo_4O_{23}$, Figure 4 (bottom))[a]

SFMO		
Fe		1.65
Mo		2.22

O^*:SFMO		
	O^*_{xy}	O^*_z
Fe(−O^*)	1.32	1.28
Mo(−O^*)	2.20	2.11
3 × Fe[b]	1.41	1.46
3 × Mo[b]	2.19	2.17

AD:SFMO

Fe/Fe$_{Mo}$	(a)		(b)		(c)	
	FM	AF	FM	AF	FM	AF
Fe$_{Mo}$	1.69	1.64	1.69	1.70	1.67	1.66
Mo$_{Fe}$	2.03	2.04	2.05	2.16	2.10	2.08
3 × Fe[b]	1.67	1.67	1.62	1.62	1.66	1.63
3 × Mo[b]	2.19	2.22	2.24	2.18	2.22	2.22

AD,O^*:SFMO

Fe/Fe$_{Mo}$	(a)				(b)				(c)	
	O^*_{Fe-xy}		O^*_{Fe-z}		O^*_{Fe-xy}		O^*_{Fe-z}		O^*_{Fe}	
	FM	AF	FM	AF	FM	AF	FM	AF	FM	AF
Fe$_{Mo}$(−O^*)	1.54	1.56	1.54	1.56	1.46	1.46	1.56	1.55	1.46	1.49
Fe(−O^*)	1.32	1.43	1.33	1.33	1.30	1.28	1.31	1.31	1.37	1.30
2 × Fe[b]	1.49	1.47	1.55	1.59	1.51	1.51	1.45	1.45	1.56	1.54
4 × Mo[b]	2.16	2.14	2.12	2.27	2.17	2.18	2.17	2.16	2.16	2.16

Fe/Fe$_{Mo}$	O^*_{Mo-xy}		O^*_{Mo-z}		O^*_{Mo-xy}		O^*_{Mo-z}		O^*_{Mo}	
	FM	AF	FM	AF	FM	AF	FM	AF	FM	AF
Mo$_{Fe}$(−O^*)	1.65	1.66	1.69	1.64	1.62	1.70	1.59	1.60	1.63	1.62
Mo(−O^*)	1.97	1.96	1.96	1.92	1.91	1.89	1.90	1.83	1.92	2.00
2 × Mo[b]	2.15	2.18	2.24	2.20	2.24	2.28	2.15	2.22	2.11	2.25
4 × Fe[b]	1.67	1.59	1.59	1.62	1.62	1.56	1.62	1.63	1.61	1.51

[a] (−O^*) indicates nearest-neighbor positions to the oxygen vacancy O^*. Fe and Mo magnetic moments are aligned antiferromagnetically and the Fe$_{Mo}$ is aligned ferromagnetically (FM) or antiferromagnetically (AF) to regular Fe atoms. [b] Average value of sites not involved in the AD.

The presence of ADs in stoichiometric SFMO results in effective charges that are essentially consistent with defect-free SFMO and depend only slightly on the FM/AF arrangement of the Fe ions. Only Mo$_{Fe}$ sites appear slightly reduced with respect to regular Mo sites. In AD:SFMO, we also observe a reorganization of the charge among the oxygen atoms of the cell, their charges ranging within −1.07e to −1.28e.
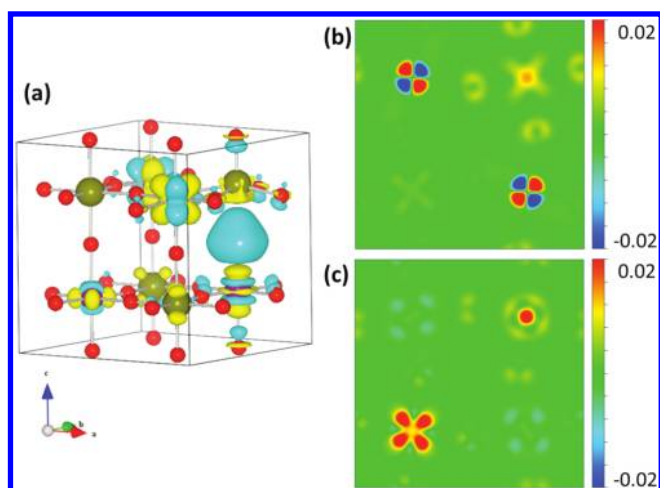
Figure 5. Charge density differences ($e \times bohr^{-3}$) upon formation of the O^*_z oxygen vacancy in SFMO (Figure 4, top). (a) 3D isosurface (Fe: purple; Mo: olive green; O: red spheres; Sr atoms are not shown for ease of viewing); yellow surface corresponds to positive values, i.e., accumulation of electrons, cyan to negative, i.e., loss of electrons. Contour slice along the (001) plane at (b) $z = 0.25$ and (c) $z = 0.75$, corresponding to the two planes of Fe/Mo cations in this representation. Plots created with the VESTA program.[33]

The presence of ADs allows the study of O vacancy formation along $Fe_{Mo}-O-Fe$ and $Mo_{Fe}-O-Mo$ bonds. Overall, we found two different behaviors. In the case of a $Mo_{Fe}-O^*-Mo$ vacancy, most of the charge remains localized and equally distributed between the Mo_{Fe} and Mo ions, while the oxygen sublattice does not receive any charge. By contrast, in the $Fe_{Mo}-O^*-Fe$ case, part of the extra charge is unevenly distributed among all the iron ions (Table 3) and a significant amount ($-0.4e$) is instead distributed among oxygen anions. These trends occur both in the FM and AF arrangements. We will return to these charge rearrangements to rationalize the results we describe next.

Next we compare structural and magnetic rearrangements that occur SFMO and AD:SFMO upon oxygen vacancy formation (Table 4). In O*:SFMO, the distance between the Fe and Mo cations closest to the O vacancy slightly increases up to 0.07 Å with respect to the original positions in the parent SFMO. In the AD,O*:SFMO cases, the cations closest to the vacancy also move away from each other up to 0.10 Å with respect to the $Fe_{Mo}-O-Fe$ and $Mo_{Fe}-O-Mo$ distances in AD:SFMO. This behavior has been also observed in other perovskite-based materials[44] and presumably is due to several effects: the larger size of the reduced cations and the lost screening by the oxygen anion produces cation–cation repulsion, as well as the loss of metal–oxo covalent bonding, probably all contribute to expanding the metal–metal distances. Regarding magnetic features, the iron atom closest to the vacancy (Fe in O*:SFMO and regular Fe in AD,O*:SFMO, which receives the highest amount of charge) exhibits a decrease in its magnetic moment (from 4.1 to ~3.7 μ_B), as expected upon reduction. For molybdenum next to an oxygen vacancy, the magnetic moment decreased from −0.5 to −0.1 to −0.2 μ_B in O*:SFMO and even becomes positive in the diagonal AD,O*:SFMO. We can understand the reduced magnetic moments on both Fe and Mo by considering that in high spin $Fe^{3+}(d^5)$ all the electrons have, for example, α spin. Therefore, to both obey the Pauli principle and preserve the magnetic balance of the system, the electron pair left behind

by the oxygen vacancy can occupy only a β spin–orbital on iron and, consequently, an α spin–orbital on molybdenum.

The electronic conductivity may be enhanced upon oxygen vacancy formation through changes in d-state occupation. As seen in Figure 2e, the presence of the oxygen vacancy does not significantly alter the electronic features of the bulk: the system retained its half-metallic nature (see also Table 4 under O*: SFMO). However, the electrons will occupy the available states of the Fe closest to the vacancy giving rise to new occupied Fe states of β character in O*:SFMO PDOS compared to SFMO PDOS (Figure 2d). As in AD:SFMO, the eigenvalue gaps in AD, O*:SFMO display a complex behavior, depending on the antisite considered and the FM/AF arrangement of Fe_{Mo} and Fe. What it is clear from these data in Table 4 is that the half-metallic nature of SFMO is not preserved in all instances of AD,O*:SFMO. Thus, although low concentrations of oxygen vacancies retain the overall electronic properties of the defect-free SFMO, ADs (combined or not with oxygen vacancies) do significantly affect the electronic structure, potentially increasing the electronic conductivity of material because the band gaps may be very small or zero. No magnetic order will persist at SOFC operating temperatures, so the differences between AF and FM states will be washed out. However, we caution that analysis of the eigenvalue gaps and magnetic moments provides only a qualitative description of these subtle electronic phenomena.

We next consider trends in oxygen vacancy formation energies for defect-free and AD:SFMO. First, we predict that oxygen vacancies in defect-free SFMO cost ~4.0 eV to form (Table 4), much higher than the cost to form ADs. Thus ADs are much more likely to form in SFMO than are oxygen vacancies. Comparing this result to values predicted by similar methods for other MIEC cathode materials, this energy of formation is quite high compared to, for example, 1−2 eV in $Ba_{(1-x)}Sr_xCo_{(1-y)}Fe_yO_3$.[47] However, once the ADs form in SFMO, the oxygen vacancy formation energy changes as a function of the local surroundings in the AD:SFMO. We predict that formation energies of oxygen vacancies along Fe−O−Fe bonds are considerably smaller: ~3.0−3.5 eV for both FM and AF arrangements. By contrast, removing an oxygen atom from Mo−O−Mo bonds costs ~4.5− 5.0 eV. It is clear that the formation of O vacancies is significantly more favorable near iron ions rather than near molybdenum ions. Consistent with this finding is the fact that the Fe−O*−Fe formation energy is predicted to be ~1 eV lower in energy than the Fe−O−Mo one in defect-free SFMO. Accordingly, the probability of forming an oxygen vacancy follows the trend Fe−O*− Fe > Fe−O*−Mo > Mo−O*−Mo. The reasons behind this trend can be found by considering the processes involved in the formation of an oxygen vacancy: the breaking of transition metal−oxygen bonds and the reorganization of the electronic structure. Indeed, the predicted oxygen vacancy formation energy trend is supported by the well-known fact that early transition metals, such as Mo, make much stronger metal−oxide bonds than midlate transition metals do, such as Fe.[48]

Further insight can be derived by considering the features of the electronic density distribution upon removal of the neutral oxygen atom. When an oxygen vacancy is created along a Mo−O−Mo_{Fe} bond, we saw that the electrons left behind remain localized among the neighboring Mo atoms, leaving the rest of the electronic density almost unchanged. By contrast, in the Fe−O*−Fe_{Mo} case, a significant amount of electron density was observed to delocalize onto the oxygen sublattice: this delocalization diminishes the electronic repulsion and helps to

Table 4. DFT-PBE+U ($(U\text{-}J)_{Fe}$= 4 eV) Structural, Magnetic, And Electronic Features (see definitions in Table 1) of SFMO with Oxygen Vacancies (O*:SFMO) and SFMO with Antisite Defects and Oxygen Vacancies (AD,O*:SFMO); and Formation Energies, E_f, of Oxygen Vacancies (O*)^a

	O*:SFMO	
	O^*_{xy}	O^*_z
d(Fe$-$O*$-$Mo) (Å)	4.03	4.08
M(Fe ($-$O*)) (μ_B)	3.71	3.72
M(Mo($-$O*)) (μ_B)	-0.10	-0.18
M_s/f.u. (μ_B)	3.51	3.54
gap (α) (eV)	1.82	1.71
gap (β) (eV)	0.00	0.00
E_f(eV)	3.94	4.01

	AD,O*:SFMO									
	(a)				(b)				(c)	
	O^*_{Fe-xy}		O^*_{Fe-z}		O^*_{Fe-xy}		O^*_{Fe-z}		O^*_{Fe}	
Fe/Fe$_{Mo}$	FM	AF	FM	AF	FM	AF	FM	AF	FM	AF
d(Fe$_{Mo}-$O*$-$Fe) (Å)	4.04	4.04	4.07	4.07	4.12	4.12	4.13	4.13	4.04	4.04
M(Fe$_{Mo}$($-$O*)) (μ_B)	4.15	-4.07	4.17	-4.06	4.13	-4.10	4.11	-4.06	3.85	-4.10
M(Fe($-$O*)) (μ_B)	3.80	3.52	3.83	3.78	3.81	3.61	3.68	3.78	3.80	3.62
M_s/f.u. (μ_B)	4.60	2.46	4.76	2.35	3.65	1.28	3.70	1.17	3.58	1.18
gap (α) (eV)	0.00	0.21	0.00	0.06	0.22	0.10	0.09	0.07	0.95	0.20
gap (β) (eV)	0.25	0.26	0.00	0.17	0.16	0.10	0.12	0.17	0.00	0.00
E_f(eV)	3.18	3.38	3.23	3.54	3.02	3.15	3.16	3.30	3.14	3.17

	O^*_{Mo-xy}		O^*_{Mo-z}		O^*_{Mo-xy}		O^*_{Mo-z}		O^*_{Mo}	
Fe/Fe$_{Mo}$	FM	AF	FM	AF	FM	AF	FM	AF	FM	AF
d(Mo$_{Fe}-$O*$-$Mo) (Å)	4.06	4.06	4.11	4.11	4.00	4.00	4.04	4.04	4.02	4.02
M (Mo$_{Fe}$($-$O*)) (μ_B)	0.53	0.94	0.80	0.79	-0.87	-0.57	-0.94	-0.84	-1.00	-0.84
M(Mo($-$O*)) (μ_B)	0.02	0.01	0.07	0.05	-0.07	-0.07	-0.22	-0.23	-0.45	-0.06
M_s/f.u. (μ_B)	4.68	2.39	4.71	2.36	3.98	1.78	3.98	1.58	3.89	2.04
gap (α) (eV)	0.00	0.03	0.07	0.20	0.30	0.13	0.00	0.25	0.07	0.06
gap (β) (eV)	0.12	0.14	0.37	0.08	0.00	0.11	0.12	0.00	0.00	0.00
E_f(eV)	4.57	4.82	4.76	4.86	4.89	4.77	5.03	5.03	4.79	4.72

^{a} Labels are defined in Figure 4. ($-$O*) indicates nearest-neighbor positions to the oxygen vacancy O*.

stabilize the vacancy. We can rationalize the origin of these two different behaviors by considering the local electronic structure of the transition metal cations. In the case of defect-free SFMO, the electronic configuration of Fe ions (roughly high spin d^5) allows the electrons left behind upon removal of neutral oxygen to go only to the spin minority states, which are delocalized over all the iron ions (as depicted by the β channel in Figure 2e). In the presence of ADs, the SFMO no longer reliably has half metallic character (Table 2). When an O vacancy is formed along the Mo$-$O$-$Mo$_{Fe}$ bond, the charge remains at the Mo sites because of the convenient reduction of the high oxidation state of Mo$^{(5+\delta)+}$ and the availability of empty d states. When instead the vacancy is formed along Fe$-$O$-$Fe$_{Mo}$, the valence band made of hybridized Fe(3d$_{eg}$)$-$O(2p) comes into play and the extra charge left by the vacancy is now able to better delocalize onto oxygens as well as irons, thus lowering the interelectronic repulsion of highly localized Fe d electrons. Therefore, the delocalization of the electronic density upon formation of an oxygen

vacancy nicely follows the trend of the oxygen formation energy, in the opposite direction: Mo$-$O$-$Mo$_{Mo}$ < Fe$-$O$-$Mo < Fe$-$O$-$Fe$_{Mo}$.

4. CONCLUSIONS

In the present work, we studied point defects in Sr$_2$FeMoO$_6$ (SFMO) and how they affect bulk properties, by considering the cases of the perfect crystal and the combined presence of defects like antisite defects (ADs) and oxygen vacancies (O*).

We found that use of the DFT+U method was mandatory to obtain a reliable description of this material: using the ab initio-derived $U\text{-}J$ value for iron we are able to predict structural, electronic, and magnetic properties in close agreement with measurements. Pure DFT with local or semilocal exchange-correlation functionals is not successful in doing so. Also, the transferability of ab initio-derived U and J parameters for derived from pure iron oxides was demonstrated by successful application to SFMO.

After validation of our theoretical approach, we explored properties of AD:SFMO, O*:SFMO, and AD,O*:SFMO. Structural features were not significantly affected by ADs, whereas the presence of an oxygen vacancy led to a more pronounced relaxation of its closest ions. Oxygen vacancies do not affect qualitatively the half-metallic character of defect-free SFMO, whereas the presence of ADs affects the electronic properties in a more pronounced way and limits such half-metallicity.

Formation of ADs costs little energy, with the highest computed AD formation energy being $\sim$0.5 eV for the preferred AF coupling of spins in the lattice. An AF disposition of the new Fe_{Mo} with respect to regular Fe atoms in the cell is found to be more stable than the FM one by a maximum of $\sim$0.60 eV. By contrast, the oxygen vacancy formation energy is predicted to be much higher ($\sim$4 eV) in defect-free SFMO. However, this energy is significantly reduced when ADs are present. We predict that the energy of formation of an oxygen vacancy along Fe—O—Fe bonds is significantly lower than the one along Fe—O—Mo bonds, which is itself lower than the one in the case of an Mo—O—Mo bond, consistent with known trends in metal—oxygen bond strengths (early transition metals such as Mo bind much more strongly to oxygen than late transition metals such as Fe do).

Moreover, analyzing the modification of the electron density upon the removal of a neutral oxygen atom, we find that lower oxygen vacancy formation energy between Fe ions is associated with a larger delocalization of the extra charge, reducing electron repulsion and at the same time potentially increasing electronic conductivity.

These predictions suggest that an excess of iron over molybdenum should provide an SFMO-based material with a higher concentration of oxygen vacancies than Sr_2FeMoO_6 and therefore it should be a better material for application as a SOFC electrode, including improved properties as a mixed electron ion conductor. In particular, the expected higher concentration of oxygen vacancies in the Fe-rich SFMO materials should accelerate oxide ion diffusion and may also enhance electronic conductivity, based on our observation of electron delocalization upon vacancy formation. Indeed, measurements of the improved performance of SOFCs made with $Sr_2Fe_{2-x}Mo_xO_{6-\delta}$ based materials have recently been reported.[12]

Finally, following the approach and method validated in this work, we are performing calculations on SFMO-based materials with higher Fe:Mo ratio, $Sr_2Fe_{1.5}Mo_{0.5}O_{6-\delta}$, focusing on formation and diffusion of oxygen vacancies as well as changes to electronic properties.

■ AUTHOR INFORMATION

Permanent Address
†Department of Chemistry "P. Corradini", University of Napoli Federico II, Napoli 80120, Italy

■ ACKNOWLEDGMENT

■ REFERENCES

(1) Boudghene Stambouli, A.; Traversa, E. *Renew. Sust. Energy Rev.* **2002**, *6*, 433.

(2) Sammes, N. M.; Smirnova, A.; Vasylyev., O., Eds. *Fuel Cell Technologies: State and Perspectives*; Springer: Dordrecht, The Netherlands, 2005.

(3) Steele, B. C. H.; Heinzel, A. *Nature* **2001**, *414*, 345.

(4) Rose, L.; Menon, M.; Kammer, K.; Kesler, O.; Larsen, P. H. *Adv. Mater. Res.* **2007**, *15*, 293.

(5) Jiang, S. P. *J. Mater. Sci.* **2008**, *43*, 6799.

(6) Adler, S. B. *Chem. Rev.* **2004**, *104*, 4791.

(7) Godickermeier, M. *Mixed ionic electronic conductors for solid oxide fuel cells*. PhD Thesis, Swiss Federal Institute of Technology, Zurich, Switzerland, 1996.

(8) Jacobson, A. J. *Chem. Mater.* **2010**, *22*, 660.

(9) Aguadero, A.; Alonso, J. A.; Escudero, M. J.; Daza, L. *Solid State Ionics* **2008**, *179*, 393.

(10) Kobayashi, K. I.; Kimura, T.; Sawada, H.; Terakura, K.; Tokura, Y. *Nature* **1998**, *395*, 677.

(11) Liu, G. Y.; Rao, G. H.; Feng, X. M.; Yang, H. F.; Ouyang, Z. W.; Liu, W. F.; Liang, J. K. *J. Phys.: Condens. Matter* **2003**, *15*, 2053.

(12) Liu, Q.; Dong, X.; Xiao, G.; Zhao, F.; Chen, F. *Adv. Mater.* **2010**, *22*, 5478.

(13) Chmaissem, O.; Kruk, R.; Dabrowski, B.; Brown, D. E.; Xiong, X.; Kolesnik, S.; Jorgensen, J. D.; Kimball, C. W. *Phys. Rev. B* **2000**, *62*, 14197.

(14) Serrate, D.; Teresa, J. M. D.; Ibarra, M. R. *J. Phys.: Condens. Matter* **2007**, *19*, 023201.

(15) Sarma, D. D.; Mahadevan, P.; Saha-Dasgupta, T.; Ray, S.; Kumar, A. *Phys. Rev. Lett.* **2000**, *85*, 2549.

(16) García-Landa, B.; Ritter, C.; Ibarra, M. R.; Blasco, J.; Algarabel, P. A.; Mahendiran, R.; García, J. *Solid State Commun.* **1999**, *110*, 435.

(17) Balcells, L.; Navarro, J.; Bibes, M.; Roig, A.; Martinez, B.; Fontcuberta, J. *Appl. Phys. Lett.* **2001**, *78*, 781.

(18) Shannon, R. D. *Acta Cryst. A* **1976**, *32*, 751.

(19) Tomioka, Y.; Okuda, T.; Okimoto, Y.; Kumai, R.; Kobayashi, K. I. *Phys. Rev. B* **2000**, *61*, 422.

(20) Mishra, R.; Restrepo, O. D.; Woodward, P. M.; Windl, W. *Chem. Mater.* **2010**, *22*, 6092.

(21) Kresse, G.; Furthmueller, J. *VASP the Guide.* University of Vienna: Vienna, Austria, 2003.

(22) (a) Anisimov, V. I.; Zaanen, J; Andersen, O. K. *Phys. Rev. B* **1991**, *44*, 943. (b) Anisimov, V. I.; Aryasetiawan, F.; Lichtenstein, A. *J. Phys.: Condens. Matter* **1997**, *9*, 767.

(23) (a) Mosey, N. J.; Carter, E. A. *Phys. Rev. B* **2007**, *76*, 155123. (b) Mosey, N. J.; Liao, P.; Carter, E. A. *J. Chem. Phys.* **2008**, *129*, 014103.

(24) Perdew, J. P.; Zunger, A. *Phys. Rev. B* **1981**, *23*, 5048.

(25) Perdew, J. P.; Burke, K.; Ernzerhof, M. *Phys. Rev. Lett.* **1996**, *77*, 3865.

(26) Linden, J.; Yamamoto, T.; Karppinen, M.; Yamauchi, H. *Appl. Phys. Lett.* **2000**, *76*, 2925.

(27) Nakamura, S.; Tanaka, M.; Kato, H.; Tokura, Y. *J. Phys. Soc. Jpn.* **2003**, *72*, 424.

(28) Kapusta, C.; Zajac, D.; Riedi, P. C.; Sikora, M.; Oates, C. J.; Blasco, J.; Ibarra, M. R. *J. Phys.: Condens. Matter* **2004**, *12*, 272.

(29) Herrero-Martín, J.; García, J.; Subías, G.; Blasco, J.; Sánchez, M. C. *J. Phys.: Condens. Matter* **2005**, *17*, 4963.

(30) Blöchl, P. *Phys. Rev. B* **1994**, *50*, 17953.

(31) Monkhorst, H. J.; Pack, J. D. *Phys. Rev. B* **1976**, *13*, 5188.

(32) Murnaghan, F. D. *Proc. Natl. Acad. Sci. U.S.A.* **1944**, *30*, 244.

(33) (a) Bader, R. F. W. *Atoms in Molecules—A Quantum Theory*, Oxford University Press: New York, 1990; (b) Tang, W.; Sanville, E.; Henkelman, G. *J. Phys.: Condens. Matter* **2009**, *21*, 084204.

(34) Momma, K.; Izumi, F. *J. Appl. Crystallogr.* **2008**, *41*, 653.

(35) Borges, R. P.; Thomas, R. M.; Cullinan, C.; Coey, J. M. D.; Suryanarayanan, R.; Ben-Dor, L.; Pinsard-Gaudart, L.; Revcolevschi, A. *J. Phys.: Condens. Matter* **1999**, *11*, L445.

4535

dx.doi.org/10.1021/cm201799c |*Chem. Mater.* 2011, 23, 4525–4536

(36) Stoeffler, D.; Colis, S. *J. Phys.: Condens. Matter* **2005**, *17*, 6415.

(37) Wu, X. *Phys. Rev. B* **2001**, *64*, 125126.

(38) Xiang, H. P.; Wu, Z. J.; Meng, J. *Phys. Status Solidi B* **2005**, *242*, 1414.

(39) Mandal, T. K.; Felser, C.; Greenblatt, M.; Kubler, J. *Phys. Rev. B* **2008**, *78*, 134431.

(40) (a) Koch, W.; Holthausen, M. C.; Eds. *A Chemist's Guide to Density Functional Theory*; Wiley: New York, 2001: (b) Johnson, B. G.; Gill, P. M. W.; Pople, J. A. *J. Chem. Phys.* **1993**, *98*, 5612.

(41) Saha-Dasgupta, T.; Sarma, D. D. *Phys. Rev. B* **2001**, *64*, 064408.

(42) Stoeffler, D. *Lect. Notes Phys.* **2010**, *795*, 197.

(43) Solovyev, I. V. *Phys. Rev. B* **2002**, *65*, 144446.

(44) Ogale, A. S.; Ogale, S. B.; Ramesh, R.; Venkatesan, T. *Appl. Phys. Lett.* **1999**, *75*, 537.

(45) Yamamoto, T.; Liimatainen, J.; Linden, J.; Karppinen, M.; Yamauchi, H. *J. Mater. Chem.* **2000**, *10*, 2342.

(46) Colis, S.; Stoeffler, D.; Mény, C.; Fix, T.; Leuvrey, C.; Pourroy, G.; Dinia, A.; Panissod, P. *J. Appl. Phys.* **2005**, *98*, 033905.

(47) Mastrikov, Y. A.; Kuklja, M. M.; Kotomin, E. A.; Maier, J. *Energy Environ. Sci.* **2010**, *3*, 1544.

(48) Carter, E. A.; Goddard, W. A., III. *J. Phys. Chem.* **1988**, *92*, 2109.

(49) Zhao, P.; Yu, R. C.; Li, F. Y.; Liu, Z. X.; Jin, M. Z.; Jin, C. Q. *J. Appl. Phys.* **2002**, *92*, 1942.

(50) Moritomo, Y.; Xu, S.; Akimoto, T.; Machida, A.; Hamada, N.; Ohoyama, K.; Nishibori, E.; Takata, M.; Sakata, M. *Phys. Rev. B* **2000**, *62*, 14224.

(51) Saitoh, T.; Nakatake, M.; Kakizaki, A.; Nakajima, H.; Morimoto, O.; Xu, S.; Moritomo, Y.; Hamada, N.; Aiura, Y. *Phys. Rev. B* **2002**, *68*, 035112.